

A Novel Single Fuzzifier Interval Type-2 Fuzzy C-Means Clustering With Local Information for Land-Cover Segmentation

Chengmao Wu^{ID} and Xiaokang Guo^{ID}

Abstract—In the process of land cover segmentation from remote sensing image, there are some uncertainties such as “significant difference in class density”, “different objects with same spectrum”, and “same object with different spectra”. Existing fuzzy c-means clustering is not sufficient to describe the high-order fuzzy uncertainties and cannot achieve accurate segmentation. Type-2 fuzzy set is perfect for handling with interclass multiple uncertainties, and clustering algorithm can suppress the noise of remote sensing image effectively by incorporating local information. Therefore, on the basis of integrating local information, this article proposes a robust single fuzzifier interval type-2 fuzzy local C-means clustering based on adaptive interval-valued data for land cover segmentation. First, interval-valued data modeling is performed for remote sensing data, and remote sensing features are represented as interval-valued vectors, and the robust interval-valued distance measure that can maximize the distance between interval-valued numbers is used to generate an interval type-2 fuzzy set through robust fuzzy clustering. Second, this article adopts an efficient type reduction method to seek equivalent type-1 fuzzy set adaptively, and realizes the segmentation of land cover by the principle of maximum type-1 fuzzy membership. The test results of multispectral remote sensing images show that the segmentation performance of this proposed algorithm outperforms existing state of the art adaptive interval type-2 fuzzy clustering algorithms, and it is beneficial to the interpretation of remote sensing image.

Index Terms—Fuzzy c-means clustering, fuzzy local information, interval type-2 fuzzy sets, interval-valued data, land cover segmentation.

I. INTRODUCTION

FUZZY theory, as the basis of fuzzy analysis, is constantly updated and developed. The defects of type-1 fuzzy clustering algorithm in dealing with uncertainty are gradually exposed, and type-2 fuzzy clustering algorithm has certain potential advantage in dealing with high-order uncertainty. Zadeh introduced type-2 fuzzy set (T2FS) as the extension of the concept of ordinary fuzzy set. In essence, it is a “fuzzy set”. In particular, T2FS is widely used to deal with various uncertainties in the

Manuscript received February 16, 2021; revised April 28, 2021 and May 26, 2021; accepted May 27, 2021. Date of publication June 1, 2021; date of current version June 17, 2021. (Corresponding author: Xiaokang Guo.)

The authors are with the School of Electronic Engineering, Xi'an University of Posts and Telecommunications, Xi'an 710121, China (e-mail: wuchengmao123@sohu.com; 18740462086@163.com).

Digital Object Identifier 10.1109/JSTARS.2021.3085606

clustering process [1]. Such as, Rhee and Hwang put forward type-2 fuzzy C-means algorithm (T2FCM) based on the classical fuzzy C-means (FCM). By assigning type-1 membership degree, the membership of each pattern is extended to type-2 fuzzy membership degree. In the presence of noise, T2FCM can get a more accurate cluster center than FCM [2]. Hwang and Rhee [3] proposed the so-called interval T2FCM (IT2FCM), which focuses on the representation and management of uncertainty in fuzzy membership and is related to the change of fuzzifier m . T2FS can analyze all kinds of complex uncertainties, i.e., T2FSs can describe the uncertainty of data by constructing membership intervals, which is better than type-1 fuzzy sets. It can be also used to deal with remote sensing images with multiple uncertainties [4].

However, the land cover types of remote sensing are inherently uncertain and there exist the phenomena of “different objects with same spectrum” and “same objects with different spectra”, it leads to the problems of existing remote sensing segmentation algorithm with weak robustness, low accuracy, and so on. With the development of remote sensing imaging technology, remote sensing image has the characteristics of high spatial resolution, hyperspectral resolution, and high temporal resolution. The complexity and noise diversity of remote sensing image segmentation are greatly increased. Existing remote sensing segmentation algorithms can not meet the needs of complex high resolution remote sensing data processing [5]. In addition, if the problem to be treated has high uncertainty or complexity, it can be easily dealt with by interval type-2 fuzzy logic systems (IT2FS) or interval-valued fuzzy set [6]. In view of potential advantages of interval T2FS, the application of IT2FS in clustering has emerged in large numbers. Ngo proposed to apply IT2FCM to land cover segmentation from multispectral satellite images [7]. Qiu *et al.* [8] proposed a modified IT2FCM with spatial information constraints, which is used for the segmentation of synthetic image and magnetic resonance (MR) image. Qiu *et al.* [9] also proposed an enhanced IT2FCM, which optimizes the initialization of clustering centers and type reduction. Yu *et al.* [10] applied IT2FCM earlier to solve the problem of remote sensing data processing. Mai and Ngo [11] used the spatial information between pixels to calculate the interval-valued membership degree, and proposed an improved IIT2FCM to solve the problem of land cover segmentation from multispectral satellite images. Ngo and Mai [12] proposed a

semisupervised interval type-2 fuzzy c-means clustering with spatial information constraints, and it is applied to land cover segmentation from multispectral remote sensing images. Guo and Huo [13] constructed an enhanced IT2FCM* algorithm for remote sensing image segmentation by utilizing spatial information and spectral index. Huo *et al.* [14] used spectral uncertainty and the ranking of interval numbers to construct an improved IT2FCM* algorithm to solve the problem of land cover segmentation. Zhang [15] proposed an adaptive interval type-2 fuzzy clustering (AIT2FCM) with weighted neighborhood distance, but its time complexity is very large. Xing *et al.* [16] proposed an interval type-2 fuzzy clustering with neighborhood information. Jiang *et al.* constructed a triangular fuzzy set to describe object uncertainty, and used interval-valued distance to generate interval T2FSs in view of two fuzzifiers. Thus, an enhanced interval type-2 fuzzy clustering algorithm (TFSV-IT2FCM) for high resolution remote sensing images segmentation is obtained [17].

Type reduction is the key and difficulty of type-2 fuzzy system method. Its essence is the extension of accurate operation in type-1 system, but it is usually much more complex than type-1 system and computationally expensive [18]. In the early days, Karnik Mendel (KM) algorithm was a popular method for type reduction. Its disadvantages are that the number of iterations is too many, the calculation is complex and time cost is large, and it is sensitive to the initial endpoint value [19]; Wu and Tan [20] proposed an efficient type reduction strategy by looking for equivalent type-1 fuzzy set. The key idea is to regard T2FS as the combination of multiple representative type-1 fuzzy sets, and the type reduction is simplified as how to select equivalent type-1 fuzzy sets. Based on the idea of type reduction [20], He *et al.* [18] introduced the adaptive factor and intraclass compactness measure into the type reduction process, and proposed an AIT2FCM.

In the face of remote sensing image interpretation, its inherent uncertainty has restricted the development of remote sensing image segmentation technology. The specific performance is that the gray value of ground objects in the image changes within a relatively concentrated range, while the interval valued data can reflect the variability and uncertainty of the observation data, and then can be used to describe the uncertainty and fuzziness of remote sensing image [22]. Interval-valued fuzzy set is widely used in clustering. Yu *et al.* [22] proposed to apply IVFCM to remote sensing data processing. He *et al.* [5] proposed interval-valued fuzzy c-means clustering algorithm (AIVFCM) algorithm, which not only considers the anisotropy of remote sensing data, but also considers the object ambiguity of remote sensing data, further reducing the misclassification caused by spectral aliasing. Feng *et al.* proposed a new AIVFCM, which combines the interval-valued data model with the priority adaptive method. It can adjust the interval width according to the clustering compactness measure and the boundary factor, and then determines the optimal feature set of the data [23]. Xu *et al.* [24] proposed a new fuzzy clustering algorithm, which combines adaptive interval-valued modeling, spatial information with fuzzy c-means clustering to improve the separability

of remote sensing data. He *et al.* [25] proposed the adaptive interval type-2 fuzzy clustering algorithm (AIVIT2FCM) algorithm based on interval-valued data to generate interval T2FSs. The type-2 fuzzy theory is introduced to further describe the high-order fuzzy uncertainty between classes and improves the classification accuracy.

It is worth noting that the type-2 fuzzy clustering algorithm mentioned previously does not introduce fuzzy local information into the calculation of membership degree and clustering center, while the spatial information of neighborhood pixels may be used to suppress the influence of noise on remote sensing image segmentation [26]. It can be seen that the segmentation performance of remote sensing image can be improved by utilizing local information. On the other hand, too much local information will lead to poor classification effect, loss of the details and other defects. To ensure the adaptability and antinoise robustness of the proposed algorithm for the segmentation of remote sensing image with different distribution and noise, this article introduces appropriate local information and sets the size of local window to 3×3 , which makes the proposed algorithm more suitable to effectively process various remote sensing data. In addition, to reduce the dependence of type-2 fuzzy clustering on the prior information of double fuzzifiers, many scholars have improved the double fuzzifiers interval type-2 fuzzy clustering algorithm to describe the uncertainty in the clustering; however, a single fuzzifier interval type-2 fuzzy clustering by using different distances is proposed. It not only reduces the dependence on fuzzifier, but also retains the uncertainty description of membership function, and it is applied to solve the segmentation problem of remote sensing image. In particular, a number of scholars [15], [17], [21], [25] have verified the feasibility of interval type-2 clustering with different distance measures in remote sensing image segmentation. Therefore, to reduce the dependence on two fuzzifiers in the classical interval type-2 fuzzy clustering, this paper introduces two interval-valued distances into interval type 2 fuzzy clustering, and proposes a novel single fuzzifier interval type-2 fuzzy clustering based on interval-valued data model. The main contributions of this article are summarized as follows.

- 1) The concept of single fuzzifier is applied to interval type-2 fuzzy clustering. At the same time, fuzzy local information is embedded in interval type-2 fuzzy clustering.
- 2) Two robust interval-valued distances are used to generate interval T2FSs in interval type-2 fuzzy local c-means clustering. A novel adaptive type reduction method is used to realize remote sensing image coverage segmentation.

The rest of this article is organized as follows. Section II introduces interval-valued type-2 fuzzy clustering-related algorithms. Section III analyses a series of interval-valued distances, and verifies that two important interval-valued distances have very good ability to cluster interval-valued data with overlapping clusters. Section IV proposes a novel robust interval type-2 fuzzy clustering algorithm and provides the overall implementation. Compare experimental results are reported in Section V and Section VI is the conclusion.

II. RELATED VARIANTS OF INTERVAL TYPE-2 ALGORITHM

A. Fuzzy Local Information C-Means

FCM is one of the standard fuzzy clustering procedures [27]. Its objective function is described as follows:

$$J_m(U, V) = \sum_{i=1}^n \sum_{k=1}^c u_{ik}^m d_{ik}^2 \quad (1)$$

$$\text{s.t. } \sum_{k=1}^c u_{ik} = 1, \forall i; u_{ik} \in [0, 1], \forall i, k; 0 < \sum_{i=1}^n u_{ik} < n, \forall k.$$

Where n is the number of samples; c is the number of clusters; u_{ik} is the membership degree of the i th sample belonging to the k th cluster, v_k is the center of the k th cluster, d_{ik}^2 is square Euclidean distance between sample x_i and cluster center v_k , m is fuzzifier, usually $m = 2.0$.

To improve the robustness of FCM, Krindis and Chatzis [28] proposed a **fuzzy C-means clustering** algorithm based on **local information (FLICM)**. And its objective function is described as follows:

$$J_m(U, V) = \sum_{i=1}^n \sum_{k=1}^c u_{ik}^m [d_{ik}^2 + G_{ik}] \quad (2)$$

where the definition of fuzzy factor G_{ik} is defined as follows:

$$G_{ik} = \sum_{j \in N_i, j \neq i} (1 - u_{jk})^m d_{jk}^2 / (sd_{ij} + 1). \quad (3)$$

And i, j represent current pixel x_i and its neighborhood pixel x_j , respectively; sd_{ij} represent the spatial distance between pixel x_i and pixel x_j ; N_i represent the neighborhood window around pixel x_i ; u_{jk} represent the membership degree of neighborhood pixel x_j belonging to the k th cluster.

The iterative expressions of membership degree u_{ik} and clustering center v_k are described as follows:

$$u_{ik} = \left(\sum_{q=1}^c ((d_{ik}^2 + G_{ik}) / (d_{iq}^2 + G_{iq}))^{1/(m-1)} \right)^{-1} \quad (4)$$

$$v_k = \left(\sum_{i=1}^n u_{ik}^m \right)^{-1} \cdot \sum_{i=1}^n u_{ik}^m x_i. \quad (5)$$

B. Type-2 Fuzzy Clustering

1) **Interval Type-2 Fuzzy C-Means Clustering**: In general, the interval type-2 fuzzy clustering has two fuzzifiers m_1 and m_2 , and its objective function is described as follows [3]:

$$\begin{cases} J_{m_1}(U, V) = \sum_{i=1}^n \sum_{k=1}^c u_{ik}^{m_1} d_{ik}^2 \\ J_{m_2}(U, V) = \sum_{i=1}^n \sum_{k=1}^c u_{ik}^{m_2} d_{ik}^2 \end{cases}. \quad (6)$$

This fuzzy clustering is called IT2FCM, and its upper and lower membership functions are given as follows:

$$\bar{u}_{ik} = \begin{cases} u_{ik}^{(1)}, (\sum_{q=1}^c (d_{ik}/d_{iq}))^{-1} \leq c^{-1} \\ u_{ik}^{(2)}, \text{ otherwise} \end{cases} \quad (7)$$

$$u_{ik} = \begin{cases} u_{ik}^{(1)}, (\sum_{q=1}^c (d_{ik}/d_{iq}))^{-1} \geq c^{-1} \\ u_{ik}^{(2)}, \text{ otherwise} \end{cases} \quad (8)$$

where $u_{ik}^{(1)} = (\sum_{q=1}^c (d_{ik}/d_{iq})^{\frac{2}{m_1-1}})^{-1} u_{ik}^{(2)} = (\sum_{q=1}^c (d_{ik}/d_{iq})^{\frac{2}{m_2-1}})^{-1}$.

To meet the constraint condition of upper and lower membership functions $\underline{u}_{ik} \leq \bar{u}_{ik}$, (7) and (8) are redefined

$$\begin{cases} \bar{u}_{ik} = \max\{u_{ik}^{(1)}, u_{ik}^{(2)}\} \\ \underline{u}_{ik} = \min\{u_{ik}^{(1)}, u_{ik}^{(2)}\} \end{cases}. \quad (9)$$

This upper and lower membership degrees are used to update the endpoints v_L and v_R of the cluster centers by means of KM type reduction method [19]. But its computational complexity is higher. So that, this article will use an adaptive type reduction strategy with efficient and better segmentation accuracy.

2) **Adaptive Interval T2FCM**: He *et al.* [18] proposed an AIT2FCM with single fuzzifier, which constructs interval T2FSS through **fuzzy uncertainty of distance measurement**. Its core lies in the construction of interval-valued membership and the full consideration of the influence of the width of interval-valued membership on the segmentation results.

The upper and lower membership degrees of AIT2FCM are described as follows:

$$\begin{cases} \bar{u}_k(x_i) = (\sum_{q=1}^c (d_{ik}/d_{iq})^{2/(m-1)})^{-1} \\ \underline{u}_k(x_i) = (\sum_{q=1}^c (s_{ik}/s_{iq})^{2/(m-1)})^{-1} \end{cases} \quad (10)$$

where, $1 \leq i \leq n$, $1 \leq k \leq c$, m is the single fuzzifier, $\bar{u}_k(x_i)$ and $\underline{u}_k(x_i)$ denote the upper and lower bounds of the interval-valued membership degree of data x_i belonging to the k th cluster, the interval-valued membership degree is expressed as $[\underline{u}_k(x_i), \bar{u}_k(x_i)]$, d_{ik}, s_{ik} represent the mean and maximum distance between x_i and the j th cluster, respectively, $d_{ik} = \text{mean}_{l=1}^w(d_{ik}^l)$, $s_{ik} = \text{max}_{l=1}^w(d_{ik}^l)$, where l is the number of data dimensions, d_{ik}^l is Euclidean distance between the l th dimension feature of sample x_i and cluster center v_k , which is specifically expressed as $d_{ik}^l = |x_{il} - v_{kl}|$.

In 2019, He *et al.* [25] put forward an **AIVIT2FCM** for interval-valued data. And the upper and lower bounds of interval-valued fuzzy membership degree are described as follows:

$$\begin{cases} u_k^a(\tilde{x}_i) = (\sum_{q=1}^c (d_{ij}/d_{iq})^{2/(m-1)})^{-1} \\ u_k^b(\tilde{x}_i) = (\sum_{q=1}^c (s_{ij}/s_{iq})^{2/(m-1)})^{-1} \end{cases}. \quad (11)$$

Lower and upper of membership function is given as

$$\begin{cases} \underline{u}_k(\tilde{x}_i) = \min\{u_k^a(\tilde{x}_i), u_k^b(\tilde{x}_i)\} \\ \bar{u}_k(\tilde{x}_i) = \max\{u_k^a(\tilde{x}_i), u_k^b(\tilde{x}_i)\} \end{cases} \quad (12)$$

where $\bar{u}_k(\tilde{x}_i)$ and $\underline{u}_k(\tilde{x}_i)$ denote the upper and lower bounds of the interval-valued membership degree of interval-valued data sample \tilde{x}_i to cluster center \tilde{v}_k , respectively, the interval-valued membership degree is expressed as $[\underline{u}_k(\tilde{x}_i), \bar{u}_k(\tilde{x}_i)]$, d_{ik}, s_{ik} are the mean and maximum distance between \tilde{x}_i and cluster center

\tilde{v}_k ; $d_{ik} = \text{mean}_{l=1}^w(d_{ik}^l)$, $s_{ik} = \max_{l=1}^w(d_{ik}^l)$, d_{ik}^l is Euclidean distance between the l th dimension feature of interval-valued sample \tilde{x}_i and cluster center \tilde{v}_k , which is specifically expressed as follow:

$$d_{ik}^l = ((m(\tilde{x}_{il}) - m(\tilde{v}_{kl}))^2 + (1/3) \cdot (w(\tilde{x}_{il}) - w(\tilde{v}_{kl}))^2)^{1/2} \quad (13)$$

where $m(\tilde{y}) = 0.5(\bar{y} + \underline{y})$, $w(\tilde{y}) = 0.5(\bar{y} - \underline{y})$, $\tilde{y} \in \{\tilde{x}_{il}, \tilde{v}_{kl}\}$, \bar{y} , \underline{y} are upper and lower bounds of the interval-value data \tilde{y} .

III. DISTANCE METRIC METHOD

Interval-valued distance has also become the premise of the accurate cluster analysis for interval-valued data. Given interval-valued number $\tilde{x} = [\underline{x}, \bar{x}]$ and $\tilde{y} = [\underline{y}, \bar{y}]$, Square Euclidean distance is extended to the interval-valued number, which is defined as follows:

$$D_1(\tilde{x}, \tilde{y}) = ((\underline{x} - \underline{y})^2 + (\bar{x} - \bar{y})^2)^{1/2}. \quad (14)$$

Equation (14) only uses the endpoint information of interval-valued numbers. However, the midpoint and half-range of the interval value are not fully utilized. Therefore, a new definition of interval-valued distance is constructed [29]

$$D_2(\tilde{x}, \tilde{y}) = ((m(\tilde{x}) - m(\tilde{y}))^2 + \theta(w(\tilde{x}) - w(\tilde{y}))^2)^{1/2} \quad (15)$$

where $m(\tilde{z}) = (\underline{z} + \bar{z})/2$, $w(\tilde{z}) = (\bar{z} - \underline{z})/2$, represent midpoint and half-range of interval-valued number, respectively; $\theta \in R^+$ is called the influence factor of interval width, usually $\theta = 1$.

Liem proposed an interval-valued distance considering all points in two interval-valued numbers based on double integral [30]

$$\begin{aligned} D_3^2(\tilde{x}, \tilde{y}) &= \iint_U [m(\tilde{x}) - m(\tilde{y}) + 2(\alpha w(\tilde{x}) - \beta w(\tilde{y}))]^2 d\alpha d\beta \\ &= (m(\tilde{x}) - m(\tilde{y})) + (1/3)(w^2(\tilde{x}) + w^2(\tilde{y})) \end{aligned}$$

where $U = \{(\alpha, \beta) | -1/2 \leq \alpha, \beta \leq 1/2\}$

$$\begin{aligned} D_3(\tilde{x}, \tilde{y}) &= ((m(\tilde{x}) - m(\tilde{y}))^2 \\ &\quad + (1/3) \cdot (w^2(\tilde{x}) + w^2(\tilde{y})))^{1/2}. \end{aligned} \quad (16)$$

Obviously, the definition of $D_3(\tilde{x}, \tilde{y})$ does not satisfy the condition: $D_3(\tilde{x}, \tilde{y}) = 0 \Leftrightarrow \tilde{x} = \tilde{y}$, i.e., for two completely equal interval-valued numbers, the distance is still not zero. And for any interval number \tilde{x}, \tilde{y} , there is always $D_3(\tilde{x}, \tilde{y}) > 0$.

Similarly, considering the difference between the corresponding points in two interval-valued numbers, the following definitions are given [31]:

$$\begin{aligned} D_4^2(\tilde{x}, \tilde{y}) &= \int_{-0.5}^{0.5} [(m(\tilde{x}) + 2\alpha w(\tilde{x})) - (m(\tilde{y}) + 2\alpha w(\tilde{y}))]^2 d\alpha \\ &= \int_{-0.5}^{0.5} [(m(\tilde{x}) - m(\tilde{y}) + 2\alpha(w(\tilde{x}) - w(\tilde{y})))]^2 d\alpha \end{aligned}$$

$$= (m(\tilde{x}) - m(\tilde{y}))^2 + (1/3) \cdot (w(\tilde{x}) - w(\tilde{y}))^2$$

$$D_4(\tilde{x}, \tilde{y}) = ((m(\tilde{x}) - m(\tilde{y}))^2 + (1/3) \cdot (w(\tilde{x}) - w(\tilde{y}))^2)^{1/2}. \quad (17)$$

The distance measure considers the deviation of the corresponding points in two interval-valued numbers, and the accuracy of the results is improved relatively.

Souza and Carvalho [32] defined the dissimilarity measure which named as city-block distances, this measure is an appropriate extension of Minkowski distance metric to interval-valued data \tilde{x} and \tilde{y} as

$$D_5(\tilde{x}, \tilde{y}) = |\underline{x} - \underline{y}| + |\bar{x} - \bar{y}|. \quad (18)$$

And theoretical studies indicate that the methods based on city-block distance is more robust than those based on Euclidean distance in the presence of outliers [33].

Bao [34] proposed D^p distance, which not only considers the difference between the expected values of two interval-valued numbers, but also considers the difference of their widths

$$D^p(\tilde{x}, \tilde{y}) = (|m(\tilde{x}) - m(\tilde{y})|^p + (1/3) \cdot |w(\tilde{x}) - w(\tilde{y})|^p)^{1/p} \quad (19)$$

where $p \geq 1$

$$D_6(\tilde{x}, \tilde{y}) = |m(\tilde{x}) - m(\tilde{y})| + (1/3) \cdot |w(\tilde{x}) - w(\tilde{y})|. \quad (20)$$

It can be proved that it satisfies nonnegativity and symmetry obviously. The triangle inequality is proved as follows:

$$\begin{aligned} D_6(\tilde{x}, \tilde{y}) &= |m(\tilde{x}) - m(\tilde{y})| + 1/3|w(\tilde{x}) - w(\tilde{y})| \\ &\leq |m(\tilde{x}) - m(\tilde{z})| + |m(\tilde{z}) - m(\tilde{y})| \\ &\quad + 1/3(|w(\tilde{x}) - w(\tilde{z})| + |w(\tilde{z}) - w(\tilde{y})|) \\ &= D_6(\tilde{x}, \tilde{z}) + D_6(\tilde{z}, \tilde{y}). \end{aligned}$$

Carvalho [35] simplified the directed Hausdorff distance of the interval-valued number, and a novel Hausdorff distance of interval-valued number is described as follows:

$$D_7(\tilde{x}, \tilde{y}) = \max\{|\bar{x} - \bar{y}|, |\underline{x} - \underline{y}|\}. \quad (21)$$

It can be proved that it obviously satisfies reflexivity and symmetry; The triangle inequality is proved as follows:

$$\begin{aligned} D_7(\tilde{x}, \tilde{y}) &= \max\{|\bar{x} - \bar{y}|, |\underline{x} - \underline{y}|\} \\ &\leq \max\{|\bar{x} - \bar{z}| + |\bar{z} - \bar{y}|, |\underline{x} - \underline{z}| + |\underline{z} - \underline{y}|\} \\ &\leq \max\{|\bar{x} - \bar{z}| + |\underline{x} - \underline{z}|\} + \max\{|\bar{z} - \bar{y}| + |\underline{z} - \underline{y}|\} \\ &= D_7(\tilde{x}, \tilde{z}) + D_7(\tilde{z}, \tilde{y}). \end{aligned}$$

Therefore, using two-dimension interval-valued numbers to construct a simply interval-valued dataset with noise, as shown in Fig. 1, and the interval-valued datasets are used to judge the robustness of different interval-valued distances.

The structure of single-valued dataset $x = \{x_1, \dots, x_{10}\}$ is shown in Table I. Similarly, the corresponding interval-valued

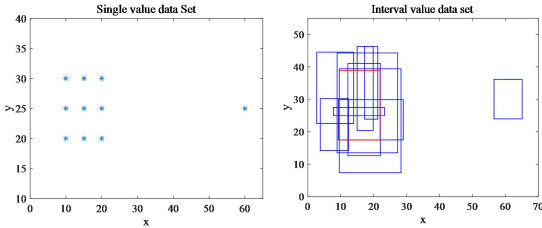


Fig. 1 Left figure shows single value dataset, right figure shows interval value dataset.

TABLE I
SINGLE VALUED DATASET

	x_1	x_2	x_3	x_4	x_5	x_6	x_7	x_8	x_9	x_{10}
dim1	10	10	10	15	15	15	20	20	20	60
dim2	30	25	20	30	25	20	30	25	20	25

TABLE II
INTERVAL VALUE DATASET

	dim1	dim2		dim1	dim2
\tilde{x}_1	[3,14]	[23,45]	\tilde{x}_6	[9,28]	[7,39]
\tilde{x}_2	[8,23]	[25,27]	\tilde{x}_7	[17,21]	[24,46]
\tilde{x}_3	[4,12]	[14,30]	\tilde{x}_8	[9,27]	[13,44]
\tilde{x}_4	[15,19]	[20,46]	\tilde{x}_9	[9,29]	[18,30]
\tilde{x}_5	[12,22]	[12,41]	\tilde{x}_{10}	[56,65]	[24,36]

dataset $\tilde{X} = \{\tilde{x}_1, \dots, \tilde{x}_{10}\}$, $\tilde{x}_i = [\underline{x}_i, \bar{x}_i]$ ($1 \leq i \leq 10$) is also constructed in Table II, where \tilde{x}_i ($1 \leq i \leq 9$) is used as the original data, and \tilde{x}_{10} is used as outlier.

The main idea to verify the robustness of each distance is to test the influence of outlier on the original data. In particular, the influence is embodied as the deviation of mean value before and after adding outlier. For the original data $\tilde{x}_i = [\underline{x}_i, \bar{x}_i]$, ($1 \leq i \leq 9$), the mean value of original data is expressed as $\tilde{v}_0 = [\underline{v}_0, \bar{v}_0]$, $\tilde{v}_0 = \text{mean}(\tilde{x}_i, 1 \leq i \leq 9)$, and then, $N(D(\tilde{x}_i, \tilde{v}_0))$ represents that interval-valued distance $D(\tilde{x}_i, \tilde{v}_0)$ are normalized to $[0, 1]$, so as to obtain the corresponding membership degree $U(u_i) = 1 - N(D(\tilde{x}_i, \tilde{v}_0))$, calculate the new mean value $\tilde{v}_{\text{new}} = [\underline{v}_{\text{new}}, \bar{v}_{\text{new}}]$, $\underline{v}_{\text{new}} = (\sum_i u_i)^{-1} \cdot (\sum_i (u_i \cdot \underline{x}_i))$, $\bar{v}_{\text{new}} = (\sum_i u_i)^{-1} \cdot (\sum_i (u_i \cdot \bar{x}_i))$, and obtain the deviation of \tilde{v}_{new} and \tilde{v}_0 is Bias = $|\tilde{v}_{\text{new}} - \tilde{v}_0| = |\underline{v}_{\text{new}} - \underline{v}_0| + |\bar{v}_{\text{new}} - \bar{v}_0|$, thus, the experimental data are obtained as follow.

According to the deviation results of each mean value in the above Table III, the order of robust performance from strong to weak is: $D_3 > D_7 > D_4 > D_1 > D_6 > D_5$, which shows that the robust performance of D_7 is better and the antinoise ability of D_6 is average. However, for a clustering method, the clustering performance is not only related to the robustness of distance measure, but also takes into account the clustering model involving distance measure. Therefore, this article still adopts the distance measure D_6, D_7 as the clustering distance of interval type-2 fuzzy clustering algorithm.

TABLE III
DEVIATION OF CLUSTER CENTER

\tilde{v}_0	$\underline{v}_0 = [9.5556, 17.3333]$	$\bar{v}_0 = [21.6667, 38.6667]$	
\tilde{v}_{new}	$\underline{v}_{\text{new}}$	\bar{v}_{new}	Bias
D_1	[9.6513, 17.2184]	[21.7684, 38.8290]	0.4751
D_3	[9.6000, 17.4733]	[21.7207, 38.4922]	0.4129
D_4	[9.6568, 17.2322]	[21.8620, 38.7177]	0.4487
D_5	[9.6911, 17.1504]	[21.9094, 38.7648]	0.6594
D_6	[9.6976, 17.2801]	[21.9428, 38.6968]	0.5015
D_7	[9.6677, 17.3251]	[21.7472, 38.8942]	0.4284

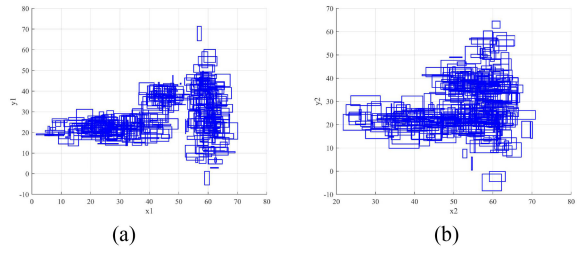


Fig. 2 Interval datasets. (a) Dataset 1 without overlapping classes. (b) Dataset 2 with overlapping classes.

TABLE IV
QUANTITATIVE EVALUATION OF DIVISION RESULTS OF DIFFERENT INTERVAL-VALUED DISTANCES

	Interval dataset 1			Interval dataset 2		
	SA	Jaccard	CR	SA	Jaccard	CR
IFCM_D1	0.7714	0.6279	0.5900	0.6171	0.4463	0.3191
IFCM_D3	0.7714	0.6279	0.5900	0.6171	0.4463	0.3191
IFCM_D4	0.7714	0.6279	0.5900	0.6171	0.4463	0.3191
IFCM_D5	0.7714	0.6588	0.6085	0.6171	0.4463	0.3191
IFCM_D6	0.7943	0.6588	0.6085	0.6200	0.4493	0.3289
IFCM_D7	0.7943	0.6588	0.6085	0.6200	0.4493	0.3226

On the other hand, to further verify the effectiveness of D_6 and D_7 distances in the classification of interval-valued dataset with serious interclass overlap, this article first constructs two different interval-valued datasets by the method in [35], where interval-valued dataset 1 has good interclass separation, and interval-valued dataset 2 has serious interclass overlap. The following Fig. 2 shows the constructed interval-valued data sets 1 and 2. Then, interval-valued fuzzy c-means clustering (IFCM) algorithms with different interval-valued distances are used to analyze them, and the SA, Jaccard, CR (the corrected Rand) indexes [35] are applied to evaluate the clustering performance of IFCM with different distance measure. From Table IV, it is seen that IFCM algorithms with D6 and D7 outperform other IFCM algorithms, and it shows that interval-valued distance such as D6 and D7 has certain potential in interval-valued dataset analysis. Therefore, interval-valued distances including D6 and D7 is selected to solve the segmentation problem of remote sensing image with serious high-order fuzzy uncertainty.

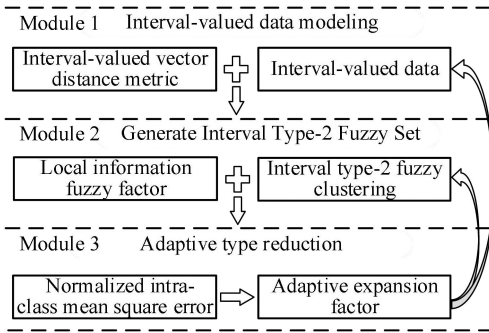


Fig. 3 Main framework of the proposed algorithm.

IV. PROPOSED ALGORITHM

A. Basic Idea of the Proposed Algorithm

As shown in Fig. 3, the algorithm proposed in this article is mainly divided into three modules. The first part is interval-valued data model, including interval-valued dataset and interval-valued distance measure; The second part is to generate interval T2FSs, which depends on interval type-2 fuzzy clustering algorithms incorporating fuzzy local information; The third part is the adaptive type reduction, which depends on the type reduction strategy with adaptive control factors.

B. Interval-Valued Data Model

In data analysis, it is difficult for single-valued variables to accurately describe and analyze samples, while interval-valued data can reflect the variability and uncertainty of observed data. Therefore, the application of interval-valued data in remote sensing image can more comprehensively reflect the spectral, spatial, and temporal characteristics of land cover.

Given the original remote sensing data x_i , the interval-value data model \tilde{x}_i is defined as follows:

$$\tilde{x}_i = [\underline{x}_i, \bar{x}_i] = [x_i - \lambda * \sigma_i, x_i + \lambda * \sigma_i] \quad (22)$$

where $x_i = (x_{i1}, \dots, x_{iw})^T$, $\sigma_i = (\sigma_{i1}, \dots, \sigma_{iw})^T$, $1 \leq i \leq n$, $1 \leq l \leq w$, x_i is original data and σ_i is the standard deviation of local information. $\lambda \in [0, 1]$ is a control factor, is also used to tune the width of the interval-valued number.

For interval-valued data, the reasonable definition of distance is also the key premise of the accurate clustering analysis. Therefore, this article uses interval-valued distance measures (20) and (21) to construct an interval type-2 fuzzy clustering algorithm for land cover segmentation.

C. Adaptive Interval Type-2 Fuzzy local Information C-Means Clustering Based on Interval-Valued Data

It is worth noting that existing interval type-2 fuzzy clustering for land cover segmentation does not embed local information, which makes it difficult to effectively solve the serious misclassification problem caused by “different objects with same spectrum” and “same object with different spectra”.

Fortunately, the algorithm based on type-2 fuzzy clustering can solve the former problem. The algorithm based on interval-valued data modeling can solve the latter problem.

Therefore, this article introduces the robust interval-valued distance into interval type-2 fuzzy clustering, and integrates fuzzy local factor of current pixel into interval-valued distance measure. In the end, a novel interval type-2 fuzzy clustering with single fuzzifier is constructed. And the optimization model of the proposed algorithm is described as (23) shown at bottom of this page, where $1 \leq i \leq n$, n is the number of samples; c is the number of clusters; and $u_k^a(\tilde{x}_i)$, $u_k^b(\tilde{x}_i)$ denote the upper and lower bounds of the interval-valued membership degree of interval-value data \tilde{x}_i belonging to cluster center \tilde{g}_k , respectively; $d^{\#,2}(\tilde{x}_i, \tilde{g}_k)$ and $s^{\#,2}(\tilde{x}_i, \tilde{g}_k)$ represents the interval-valued distance between interval-valued data \tilde{x}_i and cluster center \tilde{g}_k based on D_6 and D_7 distances, respectively; $G_{ik}^{\#}$ and $G_{ik}^{\#''}$ are two different fuzzy local factors based on robust interval-valued distance measures, which will be described in detail in the following section. Fuzzy partition membership matrix $U^a = (u_k^a(\tilde{x}_i))_{n \times c}$ and $U^b = (u_k^b(\tilde{x}_i))_{n \times c}$, cluster prototype matrix $\tilde{G} = (\tilde{g}_k)_{1 \times c}$.

1) *Initialization Method*: Initialization of cluster center: remote sensing image $X = \{x_i | 1 \leq i \leq n\}$, c is the number of clusters. At first, the gray level in the range $\min_{i=1}^n \{x_i\} \sim \max_{i=1}^n \{x_i\}$ is divided into c equal parts, the grayscale level with zero frequency number is then eliminated. Finally, the average value of pixels in each equal gray level range is used to initialize the corresponding cluster center. So, cluster center $v_k^{(0)}$ can be obtained.

Initialization of membership degree: the abovementioned initialization of cluster center $v_k^{(0)}$ is used to obtain $u_{ik}^{(0)}$ through FCM algorithm.

2) *Calculation of Cluster Center*: The upper and lower bounds $[\underline{g}_k, \bar{g}_k]$ of interval-valued cluster center \tilde{g}_k are calculated as follows:

$$\begin{aligned} \underline{g}_k &= \frac{\sum_{i=1}^n (u_{ik}^{(eq)})^m x_i}{\sum_{i=1}^n (u_{ik}^{(eq)})^m}, \\ \bar{g}_k &= \frac{\sum_{i=1}^n (u_{ik}^{(eq)})^m \bar{x}_i}{\sum_{i=1}^n (u_{ik}^{(eq)})^m} \end{aligned} \quad (24)$$

where $1 \leq k \leq c$, $u_k^{(eq)}(\tilde{x}_i)$ is represented by an initial type-1 membership degree $u_{ik}^{(0)}$ in the first iteration. $u_k^{(eq)}(\tilde{x}_i)$ is the membership degree after type reduction, and will be described in detail in the following section.

Update single-valued cluster center v_k

$$v_k = \left(\sum_{i=1}^n (u_{ik}^{(eq)})^m \right)^{-1} \cdot \sum_{i=1}^n (u_{ik}^{(eq)})^m x_i \quad (25)$$

where $1 \leq k \leq c$, $u_{ik}^{(eq)}$ is the membership degree after type reduction, and x_i is original remote sensing data.

3) *Generating T2FSs for Clustering*: For the multiobjective optimization model (23) of single fuzzifier interval type-2 fuzzy

clustering with local information constructed in this article, the upper and lower fuzzy membership degrees are derived by Lagrange multiplier method as follows.

At first, we construct the Lagrange function of the optimization model (23) with the constraint of membership degree as

$$\begin{aligned} L(U^a, U^b, \tilde{G}) = & \sum_{i=1}^n \sum_{k=1}^c (u_k^a(\tilde{x}_i))^m [d^{\#,2}(\tilde{x}_i, \tilde{g}_k) + G_{ik}^{\#,'}] \\ & + \sum_{i=1}^n \sum_{k=1}^c (u_k^b(\tilde{x}_i))^m [s^{\#,2}(\tilde{x}_i, \tilde{g}_k) + G_{ik}^{\#,''}] \\ & + \sum_{i=1}^n \lambda_i \left(1 - \sum_{k=1}^c u_k^a(\tilde{x}_i) \right) \\ & + \sum_{i=1}^n \rho_i \left(1 - \sum_{k=1}^c u_k^b(\tilde{x}_i) \right) \end{aligned} \quad (26)$$

where λ_i and ρ_i are Lagrange multiplier coefficients.

The necessary condition of this function with minimum value is as follows:

$$\begin{cases} \frac{\partial L(U^a, U^b, \tilde{G})}{\partial u_k^a(\tilde{x}_i)} = 0, \frac{\partial L(U^a, U^b, \tilde{G})}{\partial u_k^b(\tilde{x}_i)} = 0, \\ \frac{\partial L(U^a, U^b, \tilde{G})}{\partial \tilde{g}_k} = 0, \frac{\partial L(U^a, U^b, \tilde{G})}{\partial g} = 0, \\ \frac{\partial L(U^a, U^b, \tilde{G})}{\partial \lambda_i} = 0, \frac{\partial L(U^a, U^b, \tilde{G})}{\partial \rho_i} = 0. \end{cases} \quad (27)$$

By solving the abovementioned equations, we can obtain Eq. (28) shown at bottom of this page.

Upper and lower membership function are modified as

$$\begin{cases} \bar{u}_k(\tilde{x}_i) = \max(u_k^a(\tilde{x}_i), u_k^b(\tilde{x}_i)) \\ \underline{u}_k(\tilde{x}_i) = \min(u_k^a(\tilde{x}_i), u_k^b(\tilde{x}_i)) \end{cases} \quad (29)$$

where $\underline{u}_k(\tilde{x}_i)$ and $\bar{u}_k(\tilde{x}_i)$ denote the lower and upper bounds of the membership degree of sample \tilde{x}_i belonging to the k th cluster, and the interval-valued membership $[\underline{u}_k(\tilde{x}_i), \bar{u}_k(\tilde{x}_i)]$ are obtained. $d^{\#,2}(\tilde{x}_i, \tilde{g}_k)$ and $s^{\#,2}(\tilde{x}_i, \tilde{g}_k)$ denote different distance measures between sample \tilde{x}_i and cluster center \tilde{g}_k ,

respectively. Namely

$$\begin{cases} d^{\#,2}(\tilde{x}_i, \tilde{g}_k) = (D_6(\tilde{x}_i, \tilde{g}_k))^2 \\ = (|m(\tilde{x}_i) - m(\tilde{g}_k)| + 1/3 \cdot |w(\tilde{x}_i) - w(\tilde{g}_k)|)^2 \\ s^{\#,2}(\tilde{x}_i, \tilde{g}_k) = (D_7(\tilde{x}_i, \tilde{g}_k))^2 \\ = (\max\{|\tilde{x}_i - \tilde{g}_k|, |\underline{x}_i - \bar{g}_k|\})^2 \end{cases}. \quad (30)$$

The fuzzy local factor of current interval-valued number \tilde{x}_i is defined as

$$\begin{cases} G_{ik}^{\#,'} = \sum_{r \in N_i, r \neq i} (1 - \bar{u}_k(\tilde{x}_r)) d^{\#,2}(\tilde{x}_r, \tilde{g}_k) / (sd_{ri} + 1) \\ G_{ik}^{\#,''} = \sum_{r \in N_i, r \neq i} (1 - \underline{u}_k(\tilde{x}_r)) s^{\#,2}(\tilde{x}_r, \tilde{g}_k) / (sd_{ri} + 1) \end{cases} \quad (31)$$

where sd_{ri} represents the spatial distance between current \tilde{x}_i and its neighborhood interval-valued number \tilde{x}_r ; and $d^{\#,2}(\tilde{x}_r, \tilde{g}_k)$, $s^{\#,2}(\tilde{x}_r, \tilde{g}_k)$ represents different interval-valued distance measures.

4) Adaptation of Interval-Valued Data and Interval T2FSs: In the process of iteration, this article gives adaptive method for interval-valued data modeling and membership type reduction in view of clustering compactness measure [5].

The interval-valued data modeling of remote sensing data x_i is described as

$$\tilde{X}_i = [\underline{x}_i, \bar{x}_i] = [x_i - \beta_k * \sigma_i, x_i + \beta_k * \sigma_i] \quad (32)$$

where $x_i \in C_k$ ($1 \leq k \leq c$), C_k is the set of sample points belonging to the k th cluster; σ_i is the standard deviation of local information of sample point x_i ; $\beta_k \in [0, 1]$ is the contraction expansion control factor, which is used to control the width of interval-valued data.

An adaptive type reductor is described as

$$u_{ik}^{(eq)} = \bar{u}_k(\tilde{x}_i) - \beta_k \cdot [\bar{u}_k(\tilde{x}_i) - \underline{u}_k(\tilde{x}_i)] \quad (33)$$

$$\text{s.t. } \sum_{k=1}^c u_{ik}^{(eq)} = 1, 0 < \sum_{i=1}^n u_{ik}^{(eq)} < n$$

where $u_{ik}^{(eq)}$ is the equivalent type-1 membership matrix.

$$\begin{cases} \min J_1(U^a, \tilde{G}) = \sum_{i=1}^n \sum_{k=1}^c (u_k^a(\tilde{x}_i))^m [d^{\#,2}(\tilde{x}_i, \tilde{g}_k) + G_{ik}^{\#,'}] \\ \min J_2(U^b, \tilde{G}) = \sum_{i=1}^n \sum_{k=1}^c (u_k^b(\tilde{x}_i))^m [s^{\#,2}(\tilde{x}_i, \tilde{g}_k) + G_{ik}^{\#,''}] \end{cases} \quad (23)$$

$$\text{s.t. (1)} 0 \leq u_k^a(\tilde{x}_i), u_k^b(\tilde{x}_i) \leq 1, i = 1, 2, \dots, n, k = 1, 2, \dots, c;$$

$$(2) \sum_{k=1}^c u_k^a(\tilde{x}_i) = \sum_{k=1}^c u_k^b(\tilde{x}_i) = 1, i = 1, 2, \dots, n;$$

$$(3) 0 < \sum_{i=1}^n u_k^a(\tilde{x}_i), \sum_{i=1}^n u_k^b(\tilde{x}_i) < n, k = 1, 2, \dots, c$$

$$\begin{cases} u_k^a(\tilde{x}_i) = \left(\sum_{j=1}^c ((d^{\#,2}(\tilde{x}_i, \tilde{g}_j) + G_{ij}^{\#,'})) / (d^{\#,2}(\tilde{x}_i, \tilde{g}_k) + G_{ik}^{\#,'}) \right)^{1/(m-1)} \\ u_k^b(\tilde{x}_i) = \left(\sum_{j=1}^c ((s^{\#,2}(\tilde{x}_i, \tilde{g}_j) + G_{ij}^{\#,''})) / (s^{\#,2}(\tilde{x}_i, \tilde{g}_k) + G_{ik}^{\#,''}) \right)^{1/(m-1)} \end{cases} \quad (28)$$

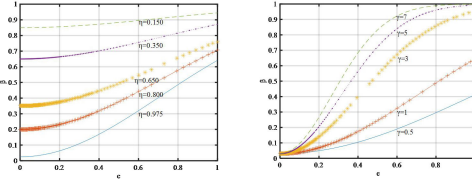


Fig. 4. (a) Influence of η on β , when $\gamma = 1$. (b) Influence of γ on β , when $\eta = 0.97$.

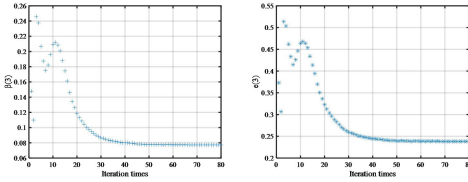


Fig. 5. (a) Curve of the control factor $\beta(3)$ with changing iteration times (the third class). (b) Curve of the normalized intraclass means square error $e(3)$ with changing iteration times (the third class).

The definition of an adaptive contraction expansion factor β_k in (30) and (31) is expressed as follows [5]:

$$\beta_k = f(e_k) = 1 - \eta * \exp(-\gamma * e_k^2) \quad (34)$$

where $\eta \in (0, 1)$, $\gamma > 0$, e_k is normalized intraclass deviation of the k th cluster, and its expression is described as follows:

$$e_k = n_k^{-1} \cdot \sum_{i \in c_k} u_{ik}^m \delta(x_i, g_k) \quad (35)$$

where u_{ik} is the membership degree of sample x_i belonging to the k th cluster; In the first iteration, u_{ik} is represented by the initial type-1 membership $u_{ik}^{(0)}$, and it is also represented by the type reduced membership $u_{ik}^{(eq)}$ in the later iterations; $\delta(x_i, g_k) = \|x_i - g_k\|$ is the deviation between sample data x_i and cluster center g_k , $g_k = (n_k)^{-1} \cdot \sum_{i \in C_k} x_i$, n_k is the number of samples belonging to the k th cluster. The influence of constant parameters λ and γ on the scaling factor β_k is shown in the figure as follows.

From Fig. 4(a) and (b), the control factor adjust the interval-value data and membership type reduction adaptively to achieve the best fuzzy partition, the control factor β_k should change rapidly with the increase of the intraclass deviation, so as to select the empirical optimal value: η is around 0.9 and γ is around 1 [5].

In the actual clustering process, the value of β_k will oscillate at the early stage, but with the increase of iteration times, the intraclass deviation tends to a minimum value, and β_k also tends to a stable value, meanwhile the type-1 membership degree tends to be stable, which means that the type reduction is completed [18]. As shown in Fig. 5, it is the test results of Hengqin by the algorithm proposed in this article.

D. Pseudocode of the Proposed Algorithm

The proposed AIVIT2FLICM algorithm.

-
- 1 Input:** Image x_i , fuzzifier m , the number of clusters c , 2 stopping error ε .
 - 3 (1) Initialization:** Initialize interval-valued data
 - 4** $\tilde{x}_i^{(0)} = [\underline{x}_i^{(0)}, \bar{x}_i^{(0)}]$ using (22); initialize cluster center $v_k^{(0)}$
 - 5** and fuzzy membership $u_{ik}^{(0)}$ using FCM algorithm; set
 - 6** initial iteration number $t = 0$; Set maximum number of
 - 7** iterations $T = 150$.
 - 8 (2) Iteration process:**
 - 9 For** $t = 1$ to T
 - 10 Step1.** Update interval-valued cluster prototype
 - 11** $\tilde{g}_k^{(t)}$: Calculate the upper and lower bounds $[\underline{g}_k^{(t)}, \bar{g}_k^{(t)}]$
 - 12** using (24).
 - 13 Step2.** Generate interval T2FSs (IT2FS):
 - 14** Calculate interval-valued distances matrices $d_{ik}^{\#,2}$ and $s_{ik}^{\#,2}$
 - 15** using (30); solve the corresponding fuzzy local factors
 - 16** $G_{ik}^{\#,1}$ and $G_{ik}^{\#,2}$ using (31); Calculate membership matrix
 - 17** $\bar{u}_k^{(t)}(\tilde{x}_i^{(t)})$, $\underline{u}_k^{(t)}(\tilde{x}_i^{(t)})$ using (29).
 - 18 Step3.** Type reduction: update control factor β_k
 - 19** using (34); Calculate the equivalent type-1 membership
 - 20** degree $u_{ik}^{(eq)}$ using (33).
 - 21 Step4.** Update interval-valued data model: Update
 - 22** interval-valued data $\tilde{x}_i^{(t+1)} = [\underline{x}_i^{(t+1)}, \bar{x}_i^{(t+1)}]$ using
 - (32);
 - 23 Step5.** Update single-valued cluster center $v_k^{(t+1)}$
 - 24** using (25).
 - 25 Step6.** Stopping criterion:
 - 26 If** $\|v_k^{(t+1)} - v_k^{(t)}\| \leq \varepsilon$ or $t \geq T$, **break**;
 - 27 Else** Set $t = t + 1$ and go to **Step 1**.
 - 28 End**
 - 29 (3) Segmentation:** Using the membership partition matrix, the label matrix is obtained by the maximum 31 membership principle.
 - 32 Output:** Segmentation image y_i , membership degree
 - 33** $u_{ik}^{(eq)}$, cluster center v_k .
-

V. EXPERIMENTAL RESULTS AND ANALYSIS

A. Data Description

To verify the superiority of this proposed algorithm, four remote sensing images are tested, and the attributes of remote sensing image are introduced in Table V, and land cover components of remote sensing image are listed in Table VI. The experiment is tested by MATLAB R2014b in Intel core i5 with 8-GB RAM. Markov random field iterated conditional modes [40], FCM [27], AIVFCM [28], FLICM [24], IT2FCM [3], AIT2FCM [18], AIVIT2FCM [25], and the proposed algorithm

TABLE V
ATTRIBUTE OF REMOTE SENSING IMAGE AND ALGORITHM PARAMETER

Dataset	Resolution (meters)	Satellite	Imaging location	Parameter Reference
Salinas	3.7	AVIRIS	Salinas Valley, California	$c=6, m=2$ [39]
Hengqin	10	SPOT5	Pearl River Delta, Zhuhai	$c=5, m=2.5$ [27,28]
Zhuhai	10	SPOT5	Coastal area of Zhuhai	$c=6, m=2.5$ [18]
PaviaU	1.3	ROSIS	Pavia, Northern Italy.	$c=6, m=2$ [39]

TABLE VI
COMPOSITION OF LAND COVER CATEGORIES IN REMOTE SENSING IMAGE

RS IMAGE	Land Cover description	
Salinas (399×429)	Vineyard-untrained	
	Grapes-untrained	
	Fallow-smooth	
	Fallow-rough-plow	
	Stubble	
	Celery	
Small Hengqin (400×400)	Unlabeled	
	Water: rivers, reservoir, raise oysters, wetland	
	Grass: arable land, lawn, weed	
	Woodland: mountain forest, artificial forest	
	Bare land: vegetable fields, garden plot, tracks	
	construction sites: golf course runway, rock	
Zhuhai (288×281)	Water: rivers, ponds	
	Woodland: natural forests, cultivated forests	
	Another green land: grassland, belts, bushes	
	Agricultural land: vegetable field, orchard, cultivated land, artificial turf	
	Buildings: building complex, construction site	
	Tidal flat: offshore beach	
PaviaU (610×340)	Meadows & trees	
	Bare soil	
	Gravel & brick	
	Asphalt & bitumen	
	Metal sheets	
	Shadows	

(AIVIT2FLICM) are tested, respectively, and after the actual segmentation test, the best fuzzifier $m \in [2, 3]$, and the size of optimal window is 3×3 . To ensure the comparability of results, set the parameters of the test-related algorithm to consistent values. The test results are shown in Fig. 6. The overall segmentation accuracy, running time, and partition coefficient are used to evaluate the performance of different algorithms. These performance indexes are described follows.

1) Partition Coefficient (PC) [36]:

$$PC = n^{-1} \cdot \sum_{i=1}^n \sum_{k=1}^c u_{ik}^2 \quad (36)$$

$PC \in [1/c, 1]$; the larger the partition coefficient is, and the better the clustering performance is.

2) XB Index (Xie and Beni) [36]:

$$V_{XB}(U, V, X, c) = \frac{\sum_{i=1}^n \sum_{k=1}^c u_{ik}^2 \|x_i - v_k\|^2}{n(\min_{k \neq s} \|v_k - v_s\|^2)} \quad (37)$$

The smaller the value $V_{XB}(c)$ is, the better the clustering performance is.

3) Segmentation Accuracy (SA) [36]:

$$SA = (\sum_{j=1}^c |C_j|)^{-1} \cdot \sum_{k=1}^c |A_k \cap C_k| \quad (38)$$

where A_k is the k th pixel set of the segmented image and C_k is the k th pixel set of the ground truth; the larger the value of SA is, the closer the segmentation result is to the ideal segmentation result.

4) Indexes of Ideal Partition Image [25]:

$$L_{ik} = \begin{cases} 1, & x_i \in k \\ 0, & \text{otherwise} \end{cases}, \hat{L}_{ik} = \begin{cases} 1, & k = \arg \max(u_{ik}) \\ 0, & \text{otherwise} \end{cases}.$$

So, we can get: $TP = \sum_{i=1}^n \sum_{k=1}^c \hat{L}_{ik} L_{ik}$; $TN = \sum_{i=1}^n \sum_{k=1}^c \bar{\hat{L}}_{ik} \bar{L}_{ik}$; $FP = \sum_{i=1}^n \sum_{k=1}^c \hat{L}_{ik} \bar{L}_{ik}$; $FN = \sum_{i=1}^n \sum_{k=1}^c \bar{\hat{L}}_{ik} L_{ik}$

$$Acc = (TP + TN) / (TP + TN + FP + FN) \quad (39)$$

$$Sen = TP / (TP + FN) \quad (40)$$

$$\text{Jaccard} = TP / (TP + FP + FN). \quad (41)$$

The larger the values of Acc, Sen, and Jaccard are, the better the segmentation performance is.

5) Kappa Coefficient [25]:

$$\text{Kappa} = (p_o + p_e) / (1 - p_e) \quad (42)$$

where p_o is the sum of the number of correctly classified samples divided by the total number of samples. The actual number of samples in each class is a_1, a_2, \dots, a_c , and predicted number of samples in each class is b_1, b_2, \dots, b_c , the number of samples is n , so $p_e = n^{-2} \cdot \sum_{l=1}^c a_l b_l$. It is distributed between 0 and 1, and the closer it is to 1, the higher the consistency is.

6) Modified Peak Signal Noise Rate (PSNR) [37]:

$$\text{PSNR} = 10 \log_{10} (255^2 / \text{MSE}) \quad (43)$$

where $\text{MSE} = n^{-1} \cdot \sum_{i=1}^n (I_1(x_i) - I_2(x_i))^2$. I_1 is the ideal segmented image and I_2 is the actual segmented image. The higher the PSNR value is, the stronger the robustness of the algorithm is.

B. Test and Analysis of Remote Sensing Image

1) *Salinas*: The first row of the Fig. 6 shows the partition results of the data collected by the 224-band AVIRIS sensor in Salinas Valley, CA, USA. The analysis shows that the spectral characteristics of each land cover classification in the data are highly similar, and all the land cover classifications in the scene are very smooth. First, Markov random field theory (MRF_ICM) is applied to segment this scene, and no satisfactory segmentation results are obtained. For example, in row 1, column (b), Grapes-untrained is almost completely classified as Celery class. FCM has achieved a good segmentation of this scenario, especially in Table VII, the kappa coefficient of FCM is 0.6293, which is second only to 0.6294 of the algorithm proposed in this article; However, In row 1, column (d), the segmentation

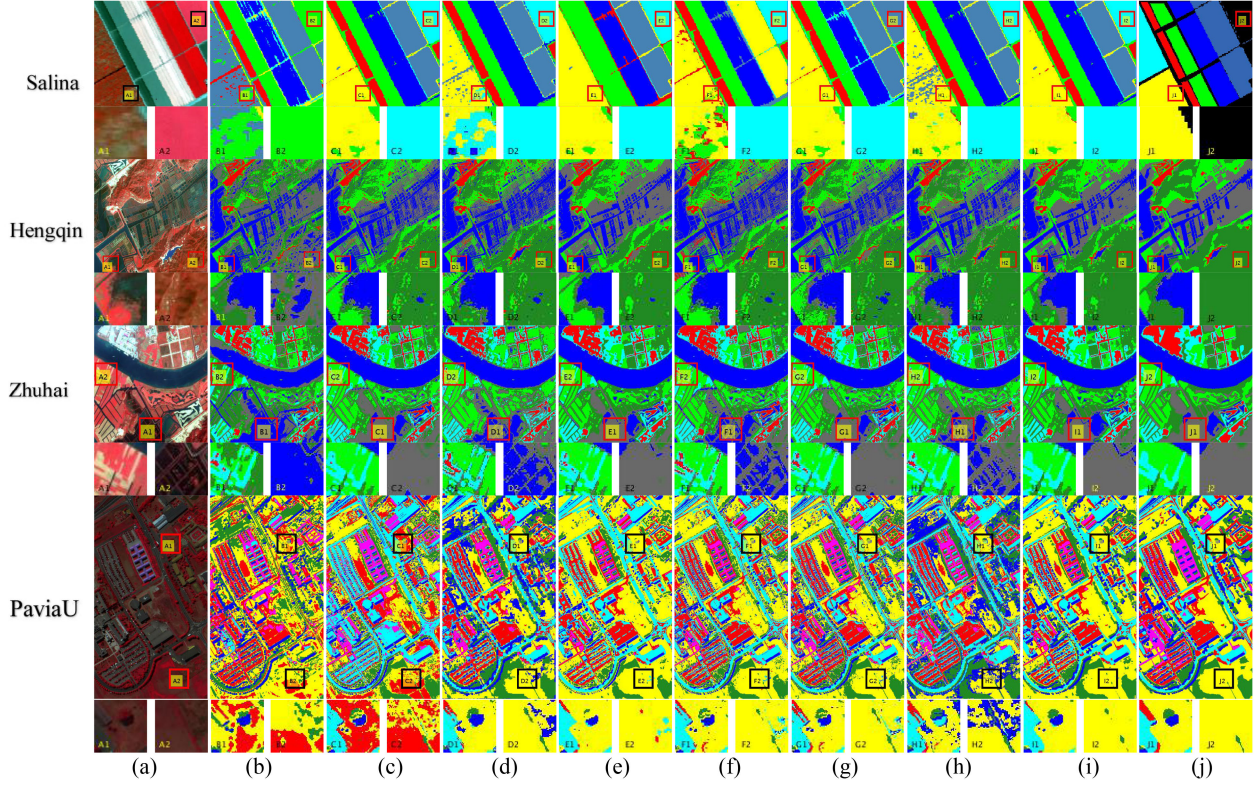


Fig. 6. Segmentation results of remote sensing images with different resolutions by different algorithms. (a) Is the original data, (b)–(i) is MRF_ICM, FCM, AIVFCM, FLICM, IT2FCM, AIT2FCM, AIVIT2FCM, and the algorithm proposed in this article. (j) Ground truth; Remote sensing images from top to bottom are Salinas, Hengqin, Zhuhai, and PaviaU.

TABLE VII
EVALUATION INDICATORS OF DIFFERENT ALGORITHMS IN REMOTE SENSING IMAGES

RS IMAGE	INDEX	MRF ICM	FCM	AIVFCM	FLICM	IT2FCM	AIT2FCM	AIVIT2FCM	PROPOSED
Salinas	PC	NULL	0.8329	0.8270	0.8888	0.7302	0.7832	0.8174	0.9004
	XB	NULL	0.0558	1.6050	0.0907	2.6512	0.0774	0.0772	0.0632
	Acc	0.8358	0.9046	0.9008	0.8853	0.8995	0.9011	0.8969	0.9046
	Sen	0.4059	0.5803	0.5635	0.4953	0.5578	0.5651	0.5463	0.5804
	Kappa	0.2686	0.6294	0.6146	0.5539	0.6125	0.6200	0.6011	0.6295
	SA	0.3230	0.6661	0.6527	0.5985	0.6482	0.6540	0.6390	0.6662
Small Hengqin	Time	17.633	2.09	20.184	16.534	20.922	20.688	28.785	14.628
	PC	NULL	0.4326	0.3276	0.5073	0.4002	0.4377	0.3738	0.5381
	XB	NULL	0.2131	0.2669	0.2007	0.2456	0.2401	0.3834	0.2393
	Acc	0.8361	0.9081	0.9019	0.9369	0.8902	0.9074	0.9134	0.9683
	Sen	0.5904	0.7702	0.7548	0.8423	0.7254	0.7685	0.7834	0.9207
	Kappa	0.4557	0.7000	0.6823	0.7914	0.6451	0.6973	0.7156	0.8953
Zhuhai	SA	0.5904	0.7702	0.7548	0.8423	0.7254	0.7685	0.7834	0.9207
	Time	12.854	4.48	32.91	97.55	73.69	21.36	32.84	233.67
	PC	NULL	0.4412	0.3548	0.5149	0.4114	0.4407	0.4285	0.5152
	XB	NULL	0.3453	2.9054	0.2694	1.0927	0.3702	0.4143	0.2691
	Acc	0.8500	0.9383	0.8844	0.9531	0.9183	0.9357	0.9275	0.9553
	Sen	0.5049	0.7592	0.5998	0.8110	0.6932	0.7510	0.7279	0.8194
PaviaU	Kappa	0.5009	0.8323	0.6380	0.8855	0.7626	0.8232	0.7933	0.8927
	SA	0.5913	0.8599	0.6967	0.9050	0.8013	0.8523	0.8274	0.9110
	Time	7.195	2.40	17.12	30.05	34.52	11.43	17.84	132.31
	PC	NULL	0.5085	0.4857	0.6417	0.6234	0.5396	0.5460	0.6317
	XB	NULL	0.4158	0.3744	0.1950	1.4214	0.1934	0.4068	0.2187
	Acc	0.8255	0.8850	0.8925	0.9091	0.9165	0.9198	0.8557	0.9276
Salinas	Sen	0.3700	0.5608	0.5992	0.6428	0.6648	0.6754	0.4856	0.7086
	Kappa	0.2260	0.4724	0.5152	0.5518	0.5847	0.5999	0.3901	0.6376
	SA	0.3700	0.5608	0.5992	0.6428	0.6648	0.6754	0.4856	0.7086
	Time	21.746	15.577	25.407	26.896	33.812	26.413	37.555	95.608

effect of AIVFCM is worse than that of FCM, and the analysis is that local information is not used in AIVFCM; FLICM loses the correct information of Fallow-smooth class after introducing local information, but it plays a very good role in suppressing noise in the partition of other classes; The segmentation result of IT2FCM is similar to that of MRF_ICM, and the same misclassification occurs. Compared with IT2FCM, AIT2FCM with adaptive type reduction has corrected the misclassification of IT2FCM. The AIVIT2FCM algorithm has noise generalization in the marked area (H1), which leads to the deterioration of the segmentation result. Therefore, based on the previous algorithm, this article introduces local information into interval type-2 fuzzy clustering algorithm with interval-valued models, and obtains the test results, which are closest to the ideal segmentation image; On the other hand, in the quantitative analysis of Table VII, under the premise of setting the same parameters of these algorithms, all indexes of the proposed algorithm are superior to other comparison algorithms, especially the SA value and Kappa coefficient are more prominent, but the disadvantage is that the proposed algorithm is time consuming.

2) *Hengqin*: The segmentation result of small Hengqin can be obtained from row 2 of Fig. 6. The visual effect of MRF_ICM used in this scene is poor, for example, the marked area (B1) in the second row 2 column(b), its woodland and grass area cannot be separated; In the marked area (B2), the dark pixels belonging to forest land are misclassified as water bodies, which indicates that the phenomenon of “same object with different spectra” related to forest land cannot be solved. FCM cannot distinguish land cover with overlapping spectra, e.g., in the marked area (C1), part of the woodland is misclassified as grassland, the mountain shadow in the marked area (C2) is misclassified as water body, and the edge of a small lake like the reservoir is misclassified as bare land, resulting in the area of reservoir is less than its actual area. In the marked area (D1), which show that AIVFCM has less misclassification of woodland and grassland, and the bare land and water at the edge of small reservoir can be correctly distinguished. FLICM can effectively suppress the spots in the marked area (E2), but the small reservoir is completely misclassified as bare land. In Fig. 6, row 2, column (f), compared with FCM, IT2FCM cannot improve the misclassification of AIT2FCM can correctly classify woodland and grassland in Fig. 6(F1), but the shadow part of the marked area (G2) is misclassified as water body. AIVIT2FCM can accurately separate woodland and other green space in the marked area (H1), and it has obvious effect on shadow removal in the marked area (H2). However, AIVIT2FCM still blurs all kinds of boundary partition and produces many noise points to interfere with boundary partition. However, the proposed algorithm with fuzzy local information constraints can suppress noise and enhance the boundary partition, there are few wrong-segmentation in the marked areas (H1, H2). In addition, the evaluation results of different algorithms for small Hengqin are shown in Table VII. As can be seen from Table VII, the proposed algorithm has the highest SA and kappa values, and other evaluation indexes also have obvious advantages. Therefore, the proposed algorithm can more effectively improve the accuracy of land cover segmentation.

3) *Zhuhai*: The segmentation result of Zhuhai can be obtained from the row 3 in Fig. 6. The visual effect of MRF_ICM used in this scene is poor, such as the marked area (B1) in the column (b), and the woodland and grassland areas cannot be separated; In the marked area (B2), the Tidal flat is misclassified as water bodies, which indicates that the phenomenon of “different objects with same spectrum” associated with water bodies cannot be solved. In the marked the area (C1), a small part of agricultural land is misclassified as buildings via FCM, while in the marked the area (C2), Only a small beach is misclassified as water body. The results of AIVFCM are worse than those of FCM in two marked areas. Compared with FCM, FLICM has better segmentation performance, stronger antinoise ability and more accurate boundary segmentation ability. In the marked the area (F1, F2), IT2FCM does achieve the correct partition for two marked areas. Compared with IT2FCM, the segmentation accuracy of AIT2FCM in the marked area (G2) is improved to a certain extent. AIVIT2FCM cannot classify the overlapping area correctly. The results of the proposed algorithm are shown in the marked area (I1, I2). The misclassification of two marked regions is obviously reduced. In addition, it can be seen from Table VII, the SA and kappa indexes of the proposed algorithm are obviously better than those of other algorithms. These test and analysis results show that the proposed algorithm can improve the segmentation results of high-resolution remote sensing images.

4) *PaviaU*: From the row 4 of Fig. 6 above, we obtain the partition result of hyperspectral data from ROSIS optical sensor. First, it is stated that to reduce the computational complexity, all kinds of features are simplified and merged, and finally we choose six types of features as the main components. At the same time, in this scene, there is a complex ground object coverage distribution, and the spectral difference between different categories is small, and there are many local “same object with different spectra”. The experimental results of each algorithm are analyzed: for the result of MRF_ICM, there are mixed points between Bare soil class and Gravel and brick class in the identified areas B1 and B2 in row 4 column (b), which indicates that the algorithm cannot distinguish the features of similar spectra; For the result of FCM, as shown in row 4, column (c), there is mixed classification between Bare soil class and Gravel and brick class, and mixed classification between Asphalt and bitumen class and Gravel and brick class outside the marked area. On the whole, the overall accuracy SA of FCM in Table VII is almost 20% higher than that of MRF_ICM. Compared with FCM, the segmentation result of AIVFCM solves the misclassification phenomenon in the marked areas D1 and D2. Then, for the result of FLICM, it is correctly classified in the identification areas E1 and E2, and the overall segmentation accuracy SA is improved by 4% compared with the previous algorithm; IT2FCM can be correctly classified the identification areas F1 and F2. Compared with FLICM, IT2FCM has the stronger ability to deal with high-order fuzzy uncertainty, so that the Kappa coefficient is improved by 2% compared with that of FLICM algorithm. Compared with IT2FCM, AIT2FCM with adaptive type reduction has a slight advantage in segmentation performance. However, for AIVIT2FCM with interval-valued

TABLE VIII
COMPUTATIONAL COMPLEXITY OF DIFFERENT METHODS

Algorithms	Computational complexity degree
MRF-ICM	$O(8nw^2l + ncl)$
FCM	$O(ncl)$
AIVFCM	$O((nc + n)l + n(2w^2 + c))$
FLICM	$O(ncw^2l)$
IT2FCM	$O((2nc + 6l'nc)l)$
AIT2FCM	$O((2nc + n)l + nc)$
AIVIT2FCM	$O((nc + 2n+)l + n(c + n + 2w^2))$
Proposed	$O((2nc + 2ncw^2 + 3n)l + n(c + 2w^2))$

TABLE IX
LABEL DESCRIPTION OF SIMPLE REMOTE SENSING IMAGE

Image	Description	Label
Residential building	Houses, buildings.	Red
	Trees, shadows.	Green
	Pavement, bare land.	Blue
The Pentagon	Trees, shadows	Red
	Bare road, Shady side of building class 1.	Green
The Pentagon	Sunny side of building class 1.	Green
	Building class 2.	Cyan

model, there is misclassification between Bare soil class and Shadows class outside the marking area. On the basis of the previous algorithm, this article adds fuzzy local information and proposes an interval type-2 fuzzy clustering method with single fuzzy factor. It makes the segmentation result smoother and the clustering effect is better than other compared algorithms. The overall accuracy rate SA is up to 70.86%, and a good visual effect is obtained. In addition, the quantitative analysis is shown in Table VII, the Kappa coefficient and total accuracy SA of the proposed algorithm are the highest when the same parameters of these algorithms are set. The test results have proved that the algorithm proposed in this article can effectively interpret hyperspectral remote sensing images and ensure high classification accuracy; The disadvantage is that the proposed algorithm needs more time.

C. Time Cost for Algorithm

The time complexity of different fuzzy clustering-related segmentation algorithms are shown in Table VIII, where n is the number of pixels in the image, c is the number of clusters, l is the number of iterations of segmentation algorithms, l' is the number of iterations of KM centroid reduction, w is the size of local window. As shown in Table VIII, this proposed algorithm has much higher time complexity.

From Fig. 7, compared with other compared algorithms, the proposed algorithm needs more time. The reason is that the proposed algorithm embedded with fuzzy local information has a great impact on time cost, but the segmentation results of the proposed algorithm is more in line with the actual coverage situation, the accuracy is improved, the visual effect is satisfactory.

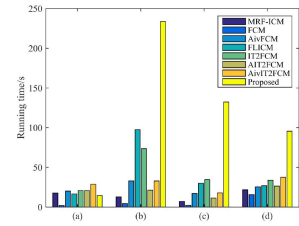


Fig. 7. Comparison of different algorithm iteration time of each test image. (a) Salinas (b) Hengqin. (c) Zhuhai. (d) PaviaU.

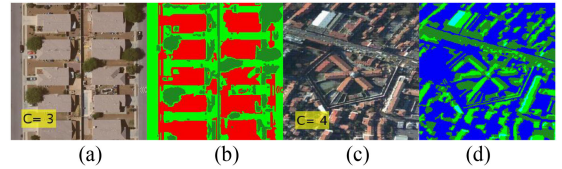


Fig. 8. Remote sensing images and ground truths. (a) Residential building. (b) Ground truth of residential building. (c) Pentagon. (d) Ground truth of the Pentagon.

D. Antinoise Performance of Algorithm

To verify the antinoise performance of the proposed algorithm, and two kinds of remote sensing images corrupted by different types of noise are selected to test the robustness of different fuzzy clustering-related algorithms in this article. The parameters are set to $m = 2$ for residential building, $m = 1.5$ for the Pentagon respectively, stopping error $\varepsilon = 10^{-5}$, and the maximum number of iterations $T = 100$.

For residential building [38] and the Pentagon in Fig. 8(a) and (c), it is corrupted by Gaussian noise of $\mu = 0$ and $\sigma = 25$, salt and pepper noise of $p = 0.15$, and speckle noise of $\sigma = 57$. These noisy images are tested by different algorithms, and their segmentation results are shown in Fig. 9, and the corresponding evaluation results are given in Table X.

As can be seen from Fig. 9, the segmentation results of the proposed algorithm are the most satisfactory and contain almost no noise. AIVIT2FLICM has strong ability to suppress salt and pepper, Gaussian or speckle noise, it has a significant advantage in suppressing different type noises. From Table X, the test results show that the proposed algorithm is superior to other comparison algorithms in different evaluation indexes, which indicates that the proposed algorithm can effectively segment remote sensing images with different types of noise in the actual environment. To further study the robust performance of different algorithms, the Pentagon image with different types and intensities of noise is used to test. The test results of different algorithms are shown in Fig. 10.

It can be seen from Fig. 10, the proposed algorithm has the largest Jaccard and Acc values, and has obvious advantages in Kappa coefficient and PSNR. With the increase of intensity of noise, the variation curves of different evaluation indexes of the proposed algorithm drop gently, which still has certain advantages compared with other fuzzy clustering-related algorithms. It happens that most high-resolution remote sensing data contain

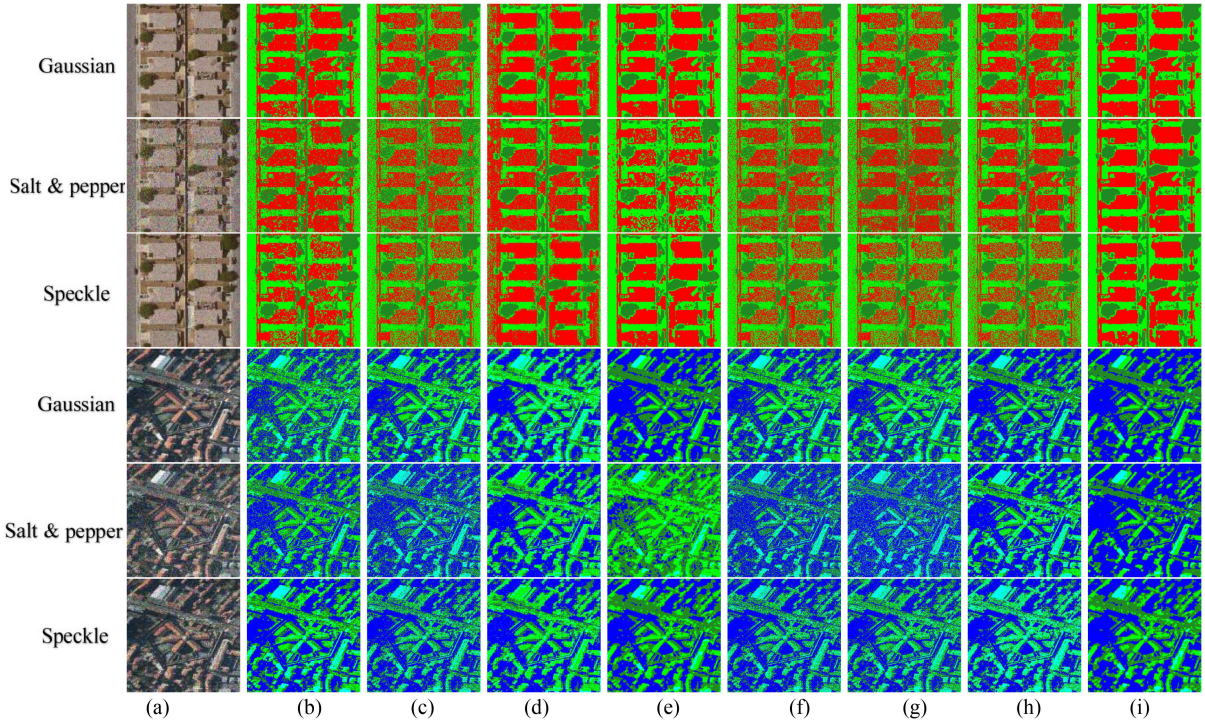


Fig. 9. Remote sensing images with noise and their segmentation results. (a)–(h) noisy image, MRF_ICM, FCM, AIVFCM, FLICM, IT2FCM, AIT2FCM, AIVIT2FCM, the proposed.

TABLE X
EVALUATION INDICATORS OF DIFFERENT ALGORITHMS FOR NOISY REMOTE SENSING IMAGE

IMAGE	NOISE	INDEX	MRF_ICM	FCM	AIVFCM	FLICM	IT2FCM	AIT2FCM	AIVIT2FCM	PROPOSED
Residential building	Gaussian (0.25)	PC	NULL	0.6223	0.6724	0.7443	0.6141	0.6081	0.7482	0.7810
		Acc	0.9300	0.8730	0.8747	0.9789	0.8745	0.8598	0.9073	0.9792
		Jaccard	0.8099	0.6799	0.6836	0.9386	0.6832	0.6525	0.7559	0.9395
		Kappa	0.8344	0.8095	0.7010	0.9497	0.7055	0.6726	0.7802	0.9504
		PSNR	13.0327	10.1535	9.8836	17.6589	10.2125	9.7653	11.2725	18.4604
	Pepper and salt (0.15)	PC	NULL	0.6656	0.6172	0.5256	0.7006	0.6376	0.6531	0.7312
		Acc	0.8573	0.7963	0.8388	0.8995	0.8109	0.7836	0.8917	0.9686
		Jaccard	0.6473	0.5319	0.6105	0.7381	0.5580	0.5098	0.7204	0.9101
		Kappa	0.6662	0.5243	0.6490	0.7611	0.5575	0.5051	0.7146	0.9256
		PSNR	10.4648	8.8371	8.8071	11.0035	9.0548	8.9820	10.8396	16.9598
	Speckle (57)	PC	NULL	0.6053	0.6458	0.7215	0.6780	0.5892	0.7278	0.7515
		Acc	0.8985	0.8348	0.8768	0.9665	0.8391	0.8288	0.8314	0.9666
		Jaccard	0.7357	0.6029	0.6880	0.9043	0.6112	0.5914	0.5963	0.8883
		Kappa	0.7604	0.6159	0.7063	0.9202	0.6249	0.6024	0.6037	0.9263
		PSNR	10.8302	8.8914	9.9868	15.0790	8.9150	8.6989	8.2786	15.1029
The Pentagon	Gaussian (0.25)	PC	NULL	0.7548	0.8241	0.8813	0.6132	0.7538	0.8257	0.8907
		Acc	0.8625	0.7867	0.7644	0.9657	0.7910	0.7647	0.8660	0.9682
		Jaccard	0.5518	0.4149	0.3839	0.8597	0.4234	0.3726	0.6034	0.8682
		Kappa	0.5303	0.3707	0.3216	0.8882	0.3817	0.3156	0.5840	0.8959
		PSNR	11.3080	9.6750	9.2407	17.3018	9.7605	9.2522	11.3882	17.6117
	Pepper and salt (0.15)	PC	NULL	0.7872	0.7408	0.6300	0.6703	0.5643	0.7555	0.8540
		Acc	0.8667	0.8059	0.8322	0.6899	0.8075	0.7905	0.8271	0.9457
		Jaccard	0.5645	0.4817	0.5224	0.2274	0.4792	0.4555	0.5196	0.7974
		Kappa	0.5497	0.4047	0.4946	0.1380	0.4027	0.3579	0.4804	0.8196
		PSNR	10.3620	8.7810	10.9257	7.9805	8.8589	8.4573	10.8224	14.7982
	Speckle (114)	PC	NULL	0.7306	0.6716	0.8142	0.5947	0.7108	0.7227	0.8280
		Acc	0.8541	0.7970	0.7936	0.9106	0.8019	0.7843	0.7809	0.9195
		Jaccard	0.5282	0.4440	0.4566	0.6911	0.4545	0.4167	0.4351	0.7203
		Kappa	0.5004	0.3741	0.3885	0.7198	0.3851	0.3491	0.3611	0.7459
		PSNR	11.0855	9.6333	9.3187	13.4983	9.7380	9.3731	9.1007	14.1094

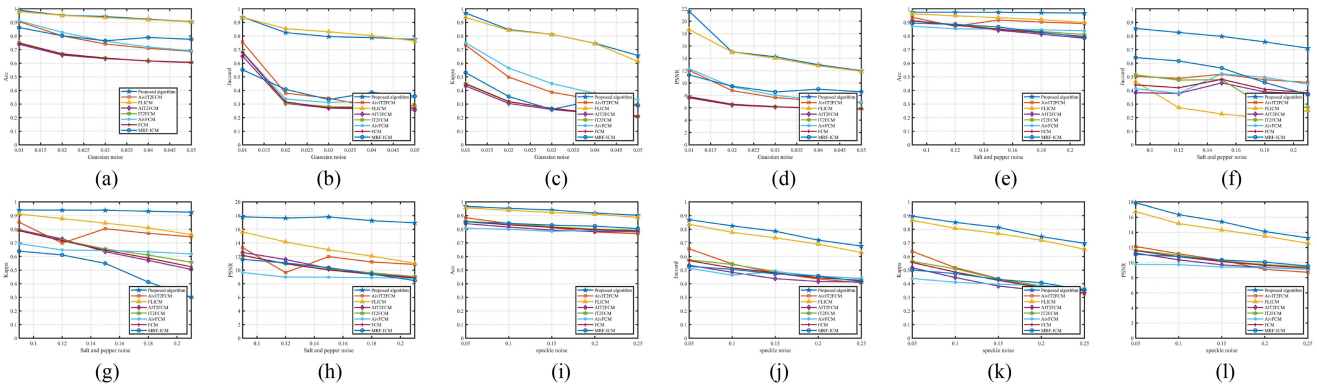


Fig. 10. (a)–(d), (e)–(h), (i)–(l), are the variation curves of each performance index in the presence of Gaussian noise, salt and pepper noise, and speckle noise, respectively. The evaluation indexes are as follows: partition accuracy Acc; Jaccard coefficient; Kappa coefficient; Peak signal-to-noise ratio PSNR.

salt and pepper or speckle noise. The proposed algorithm in this article has an outstanding ability to suppress these kinds of noise. Therefore, the proposed algorithm is more suitable to interpret remote sensing image in real environment.

VI. CONCLUSION

This article proposes a novel interval type-2 fuzzy clustering algorithm for remote sensing image segmentation. Through the segmentation test of four remote sensing images with complex ground objects, and the antinoise performance test of two simple remote sensing images with different types and intensities of noise, the effectiveness of the proposed algorithm is verified by experiments, and the following conclusions are drawn finally.

- 1) Embedding fuzzy local information makes the algorithm have high time complexity, but good segmentation performance can make up for this shortcoming.
- 2) Interval-valued data model can better solve the problem of “same object with different spectra”.
- 3) Interval valued distance can improve the classification of interclass overlapping.
- 4) The self-adaptive adjustment factor can achieve more effective and accurate fast type reduction and make the segmentation result more accurate.

Finally, the quantitative evaluation result in the experimental part also verifies the effective segmentation ability and antinoise robustness of the proposed algorithm, which shows that the proposed algorithm can obtain satisfactory segmentation results for complex remote sensing images with similar or overlapping spectra, and it can keep good effect on the image corrupted by noise in practical application.

REFERENCES

- [1] P. D’Urso, “Informational paradigm, management of uncertainty and theoretical formalisms in the clustering framework: A review,” *Inf. Sci.*, vol. 400/401, pp. 30–62, Aug. 2017, doi: [10.1016/j.ins.2017.03.001](https://doi.org/10.1016/j.ins.2017.03.001).
- [2] F. Chung, H. Rhee, and C. Hwang, “A type-2 fuzzy C-means clustering algorithm,” in *Proc. 20th NAFIPS Int. Conf. IFS World Congr.*, 2001, pp. 1926–1929, doi: [10.1109/NAFIPS.2001.944361](https://doi.org/10.1109/NAFIPS.2001.944361).
- [3] C. Hwang and F. Rhee, “Uncertain fuzzy clustering: Interval type-2 fuzzy approach to C-means,” *IEEE Trans. Fuzzy Syst.*, vol. 15, no. 1, pp. 107–120, Feb. 2007, doi: [10.1109/TFUZZ.2006.889763](https://doi.org/10.1109/TFUZZ.2006.889763).
- [4] H. Huo, J. Guo, Z. Li, and X. Jiang, “Remote sensing of spatiotemporal changes in wetland geomorphology based on type 2 fuzzy sets: A case study of beidagang wetland from 1975 to 2015,” *Remote Sens.*, vol. 9, no. 7, p. 683, Jul. 2017, doi: [10.3390/rs9070683](https://doi.org/10.3390/rs9070683).
- [5] H. He, T. Liang, D. Hu, and X. Yu, “Remote sensing clustering analysis based on object-based interval modeling,” *Comput. Geosci.*, vol. 94, pp. 131–139, Jun. 2016, doi: [10.1016/j.cageo.2016.06.006](https://doi.org/10.1016/j.cageo.2016.06.006).
- [6] C. Oscar, S. Mauricio, G. Claudia, and M. Gabriela, “Review of recent type-2 fuzzy image processing applications,” *Information*, vol. 8, no. 3, p. 97, Jun. 2017, doi: [10.3390/info8030097](https://doi.org/10.3390/info8030097).
- [7] L. T. Ngo and D. D. Nguyen, “Land cover classification using interval type-2 fuzzy clustering for multi-spectral satellite imagery,” in *Proc. IEEE Int. Conf. Syst.*, Oct. 2012, pp. 2371–2376, doi: [10.1109/ICSMC.2012.6378097](https://doi.org/10.1109/ICSMC.2012.6378097).
- [8] C. Qiu *et al.*, “A modified interval type-2 fuzzy c-means algorithm with application in MR image segmentation,” *Pattern Recognit. Lett.*, vol. 34, no. 12, pp. 1329–1338, Sep. 2013, doi: [10.1016/j.patrec.2013.04.021](https://doi.org/10.1016/j.patrec.2013.04.021).
- [9] C. Qiu *et al.*, “Enhanced interval type-2 fuzzy c-means algorithm with improved initial center,” *Pattern Recognit. Lett.*, vol. 38, pp. 86–92, Mar. 2014, doi: [10.1016/j.patrec.2013.11.011](https://doi.org/10.1016/j.patrec.2013.11.011).
- [10] X. Yu, W. Zhou, and H. He, “A method of remote sensing image auto classification based on interval type-2 fuzzy c-means,” in *Proc. IEEE Int. Conf. Fuzzy Syst.*, Sep. 2014, pp. 223–228, doi: [10.1109/FUZZ-IEEE.2014.6891759](https://doi.org/10.1109/FUZZ-IEEE.2014.6891759).
- [11] S. D. Mai and L. T. Ngo, “Interval type-2 fuzzy c-means clustering with spatial information for land-cover classification,” in *Intelligent Information and Database Systems*, N. Nguyen, B. Trawiński, and R. Kosala, Eds., vol. 9011, Switzerland: Springer, 2015, pp. 387–397, doi: [10.1007/978-3-319-15702-3_38](https://doi.org/10.1007/978-3-319-15702-3_38).
- [12] L. T. Ngo and D. S. Mai, “Semi-supervising interval type-2 fuzzy c-means clustering with spatial information for multi-spectral satellite image classification and change detection,” *Comput. Geosci.*, vol. 83, pp. 1–16, Oct. 2015, doi: [10.1016/j.cageo.2015.06.011](https://doi.org/10.1016/j.cageo.2015.06.011).
- [13] J. Guo and H. Huo, “An enhanced IT2FCM* algorithm integrating spectral indices and spatial information for multi-spectral remote sensing image clustering,” *Remote Sens.*, vol. 9, p. 960, Sep. 2017, doi: [10.3390/rs9090960](https://doi.org/10.3390/rs9090960).
- [14] H. Huo, J. Guo, and Z. Li, “Hyperspectral image classification for land cover based on an improved interval type-II fuzzy c-means approach,” *Sensors (Basel)*, vol. 18, no. 2, pp. 363, Jan. 2018, doi: [10.3390/s18020363](https://doi.org/10.3390/s18020363).
- [15] A. Zhang *et al.*, “Remote sensing image change detection based on an adaptive interval type-2 fuzzy clustering,” *J. Geomatics Sci. Tech.*, vol. 35, no. 4, pp. 376–382, 2018, doi: CNKI: SUN: JF JC.0.2018-04-009.
- [16] H. Xing *et al.*, “An interval type-2 fuzzy sets generation method for remote sensing imagery classification,” *Comput. Geosci.*, vol. 133, p. 104287, Dec. 2019, doi: [10.1016/j.cageo.2019.06.008](https://doi.org/10.1016/j.cageo.2019.06.008).
- [17] T. Jiang, D. Hu, and X. Yu, “Enhanced IT2FCM algorithm using object-based triangular fuzzy set modeling for remote-sensing clustering,” *Comput. Geosci.*, vol. 118, pp. 14–26, Sep. 2018, doi: [10.1016/j.cageo.2018.05.009](https://doi.org/10.1016/j.cageo.2018.05.009).
- [18] H. He, D. Hu, and X. Yu, “Land cover classification based on adaptive interval type-2 fuzzy clustering,” *Chinese J. Geophys.*, (in Chinese), vol. 59, no. 6, pp. 1983–1993, 2016, doi: [10.6038/cjg20160505](https://doi.org/10.6038/cjg20160505).

- [19] N. N. Karnik and J. M. Mendel, "Centeroid of a type-2 fuzzy set," *Inf. Sci.*, vol. 132, no. 1–4, pp. 195–220, Feb. 2001, doi: [10.1016/S0020-0255\(01\)00069-X](https://doi.org/10.1016/S0020-0255(01)00069-X).
- [20] H. Wu and J. M. Mendel, "Uncertainty bounds and their use in the design of interval type-2 fuzzy logic systems," *IEEE Trans. Fuzzy Syst.*, vol. 10, no. 5, pp. 622–639, Oct. 2002, doi: [10.1109/TFUZZ.2002.803496](https://doi.org/10.1109/TFUZZ.2002.803496).
- [21] G. Feng *et al.*, "Remote sensing image classification via semi-supervised fuzzy c-means algorithm," *J. Comput. Appl.*, vol. 39, no. 11, pp. 3227–3232, 2019, doi: [10.1177/j.issn.1001-9081.2019051043](https://doi.org/10.1177/j.issn.1001-9081.2019051043).
- [22] X. Yu *et al.*, "Land cover classification of remote sensing imagery based on interval-valued data fuzzy c-means algorithm," *Sci. China Earth Sci.*, vol. 57, no. 6, pp. 1306–1313, Jan. 2014, doi: [10.1007/s11430-013-4689-z](https://doi.org/10.1007/s11430-013-4689-z).
- [23] G. Feng *et al.*, "A preferential interval-valued fuzzy c-means algorithm for remotely sensed imagery classification," *Int. J. Fuzzy Syst.*, vol. 21, pp. 2212–2222, Jul. 2019, doi: [10.1007/s40815-019-00706-x](https://doi.org/10.1007/s40815-019-00706-x).
- [24] J. Xu *et al.*, "Landcover classification of satellite images based on an adaptive interval fuzzy c-means algorithm coupled with spatial information," *Int. J. Remote Sens.*, vol. 41, no. 6, pp. 2189–2208, doi: [10.1080/01431161.2019.1685718](https://doi.org/10.1080/01431161.2019.1685718).
- [25] H. He, H. Xing, D. Hu, and X. Yu, "Novel fuzzy uncertainty modeling for land cover classification based on clustering analysis," *Sci. China Earth Sci.*, vol. 62, no. 2, pp. 438–450, 2019, doi: [10.1007/s11430-017-9224-6](https://doi.org/10.1007/s11430-017-9224-6).
- [26] H. Zhang *et al.*, "Enhanced spatially constrained remotely sensed imagery classification using a fuzzy local double neighborhood information c-means clustering algorithm," *IEEE J. Sel. Topics Appl. Earth Observ. Remote Sens.*, vol. 11, no. 8, Aug. 2018, doi: [10.1109/JSTARS.2018.2846603](https://doi.org/10.1109/JSTARS.2018.2846603).
- [27] J. C. Bezdek, E. Robert, and F. William, "FCM: The fuzzy C-means clustering algorithm," *Comput. Geosci.*, vol. 10, no. 2/3, pp. 191–203, 1984, doi: [10.1016/0098-3004\(84\)90020-7](https://doi.org/10.1016/0098-3004(84)90020-7).
- [28] S. Krinidis and V. Chatzis, "A robust fuzzy local information c-means clustering algorithm," *IEEE Trans. Image Process.*, vol. 19, no. 5, pp. 1328–1337, May 2010, doi: [10.1109/TIP.2010.2040763](https://doi.org/10.1109/TIP.2010.2040763).
- [29] W. Zhang and W. Liu, "Fuzzy c-means clustering algorithm for interval data," *Comput. Eng.*, vol. 34, no. 11, pp. 26–28, Jun. 2008, doi: [10.3969/j.issn.1000-3428.2008.11.010](https://doi.org/10.3969/j.issn.1000-3428.2008.11.010).
- [30] L. Tran and L. Duckstein, "Comparison of fuzzy numbers using a fuzzy distance measure," *Fuzzy Sets Syst.*, vol. 130, no. 3, pp. 331–341, Sep. 2002, doi: [10.1016/S0165-0114\(01\)00195-6](https://doi.org/10.1016/S0165-0114(01)00195-6).
- [31] X. Li and S. Zhang, "Rank of interval numbers based on a new distance measure," *J. XIHUA Univ. (Nat. Sci. Ed.)*, vol. 27, pp. 87–90, 2008, doi: [10.3969/j.issn.1673-159X.2008.01.029](https://doi.org/10.3969/j.issn.1673-159X.2008.01.029).
- [32] R. M. C. R. D. Souza and F. D. A. T. D. Carvalho, "Clustering of interval data based on city-block distances," *Pattern Recognit. Lett.*, vol. 25, no. 3, pp. 353–365, Feb. 2014, doi: [10.1016/j.patrec.2003.10.016](https://doi.org/10.1016/j.patrec.2003.10.016).
- [33] K. Jajuga, "L₁-norm based fuzzy clustering," *Fuzzy Sets. Syst.*, vol. 39, no. 1, pp. 43–50, Jan. 1991, doi: [10.1016/0165-0114\(91\)90064-W](https://doi.org/10.1016/0165-0114(91)90064-W).
- [34] Y. Bao, X. Peng, and B. Zhao, "The interval number distance and completeness based on the expectation and width," *Fuzzy Syst. Math.*, vol. 27, pp. 133–139, 2013, doi: [10.3969/j.issn.1001-7402.2013.06.021](https://doi.org/10.3969/j.issn.1001-7402.2013.06.021).
- [35] F. D. A. T. D. Carvalho, R. M. C. R. D. Souza, M. Chavent, and Y. Lechevallier, "Adaptive hausdorff distances and dynamic clustering of symbolic interval data," *Pattern Recognit. Lett.*, vol. 27, no. 3, pp. 167–179, Feb. 2006, doi: [10.1016/j.patrec.2005.08.014](https://doi.org/10.1016/j.patrec.2005.08.014).
- [36] P. K. Mishra *et al.*, "A novel type-2 fuzzy c-means clustering for brain MR image segmentation," *IEEE Trans. Cybern.*, to be published, doi: [10.1109/TCYB.2020.2994235](https://doi.org/10.1109/TCYB.2020.2994235).
- [37] Y. Guo and A. Sengur, "A novel color image segmentation approach based on neutrosophic set and modified fuzzy c-means," *Circuits, Syst. Signal Process.*, vol. 32, no. 4, pp. 1699–1723, Dec. 2012, doi: [10.1007/s00034-012-9531-x](https://doi.org/10.1007/s00034-012-9531-x).
- [38] Y. Yang and S. Newsam, "Bag-of-visual-words and spatial extensions for land-use classification," in *Proc. Sigspatial Int. Conf. Adv. Geographic Inf. Syst. ACM*, Jan. 2010, doi: [10.1145/1869790.1869829](https://doi.org/10.1145/1869790.1869829).
- [39] Data Set: [Online]. Available: http://www.ehu.eus/ccwintco/index.php?title=Hyperspectral_Remote_Sensing_Scenes
- [40] R. C. Dubes, A. K. Jain, S. G. Nadabar, and C. C. Chen, "MRF model-based algorithms for image segmentation," in *Proc. 10th Int. Conf. Pattern Recognit.*, Atlantic City, NJ, USA, 1990, pp. 808–814, doi: [10.1109/ICPR.1990.118221](https://doi.org/10.1109/ICPR.1990.118221).



Chengmao Wu received the B.S. degree in computer applications from Xi'an Technological University, Xi'an, China, in 1992.

He is currently a Senior Engineer with the School of Electronic Engineering, Xi'an University of Posts and Telecommunications, Xi'an. His research interests include digital image processing, the circuit system, and fuzzy intelligent information processing system.



Xiaokang Guo received the B.S. degree from the Xi'an University of Posts and Telecommunications, Xi'an, China, where he is currently working toward the master's degree in electronics and information science with the School of Electronic Engineering.

His research interests include automatic classification of remote sensing images and color image processing.